Kildal, P.; Zaman, AU.; Rajo Iglesias, E.; Alfonso Alós, E.; Valero-Nogueira, A. (2011). Design and experimental verification of ridge gap waveguide in bed of nails for parallel-plate mode suppression. IET Microwaves Antennas and Propagation. 5(3):262-270. doi:10.1049/iet-map.2010.0089.

Design and Experimental Verification of Ridge Gap Waveguide in Bed of Nails for Parallel Plate Mode Suppression

[1]Per-Simon Kildal, [1]Ashraf Uz Zaman, [2]Eva Rajo-Iglesias, [3]Esperanza Alfonso, [3]Alejandro Valero-Nogueira,

[1]Department of Signals and Systems, Chalmers University of Technology, SE- 41296, Göteborg, Sweden.
{ per-simon.kildal, zaman }@chalmers.se

[2]Department of Signal Theory and Communicaiton, University Carlos-III of Madrid, 28911Leganes (Madrid), Spain
eva@tsc.uc3m.es

[3] Universidad Polite´cnica De Valencia, Valencia 46022, Spain
esalal1@iteam.upv.es; avaler@dcom.upv.es

Abstract **–** This paper describes the design and experimental verification of the ridge gap waveguide, appearing in the gap between parallel metal plates. One of the plates has a texture in the form of a wave-guiding metal ridge surrounded by metal posts. The latter posts, referred to as a pin surface or bed of nails, is designed to give a stopband for the normal parallel-plate modes between 10 and 23 GHz. The hardware demonstrator includes two 90° bends and two capacitive coupled coaxial transitions enabling measurements with a VNA. The measured results verify the large bandwidth and low losses of the quasi-TEM mode propagating along the guiding ridge, and that 90° bends can be designed in the same way as for microstrip lines. The demonstrator is designed for use around 15 GHz. Still, the ridge gap waveguide is more advantageous for frequencies above 30 GHz, because it can be realized entirely from metal using milling or molding, and there are no requirements for conducting joints between the two plates that otherwise is a problem when realizing conventional hollow waveguides.

1. INTRODUCTION:

Recently a new gap waveguide technology for millimeter and sub-millimeter waves has been introduced [1]-[3]. The waveguide is generated in a narrow gap between parallel metal plates. One of the plates is textured by a periodic pattern (e.g. metal posts) that prevents global parallel plate modes from propagating. The texture also includes single metal ridges or strips or grooves forming the transmission line or waveguide along which local confined waves propagate. The gap waveguides can be realized without dielectrics, and there is no need for any metal connection between the two plates, although there may with advantage be a metal rim along the edges of the plates to support them at a constant height relative to each other. This makes it advantageous relative to existing high frequency

transmission lines, such as microstrip or coplanar lines (dielectrics needed), and conventional hollow waveguides (conducting metal joints needed). In addition, the gap waveguide can be designed to be completely enclosed, without the presence of cavity modes, which also makes it an attractive packaging technology. This packaging capability has already been demonstrated for microstrip circuits [4]. The purpose of the present paper is to describe the design and measurements of a ridge gap waveguide hardware demonstrator built for use around 15 GHz. The demonstrator is shown in Fig. 1. The previous works presented only the conceptual ideas and initial numerical results [1]-[3].

The periodic texture must create a parallel-plate cut-off band. This can be realized theoretically by providing one of the plates with high surface impedance, i.e., by making it an artificial magnetic conductor. Soft and hard surfaces [5] represent an anisotropic magnetic conductor. They can therefore also create a parallel-plate stopband, except in one direction. Actually, local confined gap waves were already experimentally verified to appear along dielectric-filled corrugated hard surfaces [6]. The soft and hard surfaces can also be realized by metal strips on a grounded substrate [7]. The original metal strip realization suffered from problems with undesirable substrate modes. This is readily solved by using wide metal strips with metalized via holes as proposed in [7]. This realization will also have lower profile than corrugations, and was inspired by the high-impedance mushroom surface [9]. The latter is an isotropic high impedance surface and will therefore also create the parallel-plate stopband. All these ways of realizing parallel-plate stopbands are compared in [10].

We have in the present work chosen a so-called bed of nails [11], referred to as a pin surface, for creating the parallel-plate stopband. The metal posts or pins can easily be casted or milled, like the ridges also can be. Such manufacturing will also allow the height of the texture to vary, thereby creating more opportunities and degrees of freedom in a design process than substrate-bound alternatives. This may open up for new solutions for antennas and waveguide components. Of special interest is the integration of active components like amplifiers and MMICs even in the form if unpackaged semiconductor chips, which should be easy, because cooling, shielding and packaging are more or less automatically provided by the gap waveguide itself.

The gap waveguides are a result of research on soft and hard surfaces, originating from [5], generalized in [12], and overviewed in [7]. The local gap waves were first observed at Technical University of Valencia and Technical University of Madrid when they studied how to design an oversized parallel plate waveguide feeding a slot array [13]-[14]. In [13] the parallel plate waveguide was formed between a smooth metal plate and another longitudinally

corrugated hard surface plate. The hard surface suppressed higher order parallel plate modes, and local single quasi-TEM waves following single ridges appeared when the structure was excited from a point source [15]. Later at Chalmers this was developed into the general gap waveguide technology [1]. It should also be mentioned that local confined waves along hard surfaces were detected already in [16], but these waves followed the grooves of corrugated surfaces, whereas the local confined waves of the gap waveguide follow the ridges.

The present paper will describe the design and characterization of the gap waveguide demonstrator for 12-18 GHz shown in Fig. 1, realized by ridge and metal pins, and including transitions from coaxial connectors to enable measurements with a vector network analyzer (VNA). The designs have been done by using the general FDTD and FEM-based Solver CST Microwave Studio (CST) [17]. The measurements included calibration using a designed TRL (Thru, Reflection, Line) calibration kit in gap waveguide technology.

2. Principle of Operation by Comparison with Other Transmission Lines and Waveguides

The gap waveguide has similarities with several other transmission lines and waveguides. It can be seen as a linearly polarized hard waveguide. The *ideal hard waveguide* in Fig. 2a consists of two horizontal perfect electric conducting (PEC) walls, and two vertical perfect magnetic conducting walls (PMC), and can support a uniform TEM field. The *ideal gap waveguide* in Fig. 2b consists of two parallel plates, one being PEC and the other PMC, and in the PMC plate there is a guiding PEC strip. The PEC/PMC regions on both sides of the PEC strip are in cut-off when the gap height $h < \lambda/4$ where λ is the wavelength. Therefore, the field propagating along the central strip will experience these two parallel-plate cut-off regions as if they were PMC boundaries, thus the similarity with the hard waveguide. There is an exponentially decaying penetration of the fields into the two parallel-plate cut-off regions, similar to how the propagating field in a hard waveguide will penetrate into all types of realizations of hard walls. The ideal linearly polarized hard waveguides can be miniaturized like the gap waveguide, meaning that the gap waveguide itself has no lower cut-off related to its width w and gap height h, as long as we are able to realize a parallel-plate cut-off. The hard waveguide can be realized both by loading two parallel walls with a dielectric substrate [17], and with a periodic texture [19], but both these realization have larger losses and much narrower bandwidth than the present gap waveguide. They also do not have any of the other advantages of the gap waveguide described in the introduction.

The parallel-plate cut-off is essential for the operation of the gap waveguide. This will ideally be present when

the lower surface is a PMC and the gap height $h < \lambda/4$. The PMC must be realized in some way, and such realizations are normally referred to as metamaterials. There have also been other attempts to make metamaterial-based waveguides, such as that reported in [21]-[22]. However, this and other related solutions make use of wave propagation inside the metamaterial, or at the surface of it, both of which causes losses and dispersion. Parallel-plate cut-off has also been reported in [20] as a way to reduce coupling in multilayer circuit boards, realized by an electromagnetic band gap (EBG) surface.

The gap waveguide has many similarities with the so-called inverted microstrip line [23], and the rectangular ridge waveguide [24], as already pointed out in [1]. Here we will stress the similarity with the stripline, as shown in Fig. 2c. The strip line consists of parallel metal plates separated by a substrate and with a metal strip halfway between the plates. The stripline has a PMC-type symmetry plane in the middle of the gap as illustrated, making it look like two opposing gap waveguides, one being an image of the other. This means that we can use the formulas for striplines in order to determine the characteristic impedance of the ideal gap waveguide, and the approximate performance of realized ones.

3. DESIGNING FOR DESIRED CHARACTERISTIC IMPEDANCE

The equivalence between the stripline and a "PMC-imaged" ideal gap waveguide is already explained above, and can be seen in Fig. 2c. Thereby, the characteristic impedance of the ideal gap waveguide is given by

$$Z = 2Z_{Stripline} \tag{1}$$

where $Z_{stripline}$ can e.g. be found in [25] to be

$$Z_{Stripline} = \frac{\eta}{4}\left(\frac{W_e}{2h} + 0.441\right)^{-1} \tag{2}$$

with

$$\frac{W_e}{2h} = \frac{W}{2h} - \begin{cases} 0 \quad , & W/(2h) > 0.35 \\ \left(0.35 - (W/(2h))\right)^2 , & W/(2h) < 0.35 \end{cases} \tag{3}$$

This formula gives a fast estimate of the characteristic impedance, but unfortunately it may not be very accurate in practice when the PMC realization is considered. Therefore, after having designed the pin surface, we calculated the final characteristic impedance of the ideal (see Fig. 2b) and realized gap waveguides, and we adjusted the ridge width to achieve 50 Ω. The ridge width could be adjusted without affecting the bandwidth of the parallel-plate cut-off. For these calculations, CST Microwave Studio was used in three ways:

a) *WP model:* Waveguide ports (WP) are located at each end of the ridge, similar to how CST can excite microstrip lines. Then, CST computes the modal field and gives the line impedance for every mode at a chosen frequency. Unfortunately, CST cannot handle ports in waveguides with a longitudinal periodicity, such as our gap waveguide with periodic pins. Therefore, we chose to locate the port in such a way that it did not cover the periodic pin region, but only the gap region above the ridge and pins, extending laterally to include 2 pin periods on both sides of the ridge. The inclusion of the periodic pin region in the port definition gave very strange results. We studied the effect of extending the port laterally more than 2 pin periods, but the changes were small. Still, not including the pin region itself is a a severe limitation so we can only expect correct result for the characteristic impedance of the ideal gap waveguide with the ridge surrounded by ideal PMCs.

b) *V/I model:* A number of E- and H-field probes are located in the transverse xy-plane (see coordinate system in Fig. 2a), at a certain z-coordinate along the ridge. The vertical y-directed E-plane probes are located along a y-directed line between the surfaces of the ridge and of the upper metal plate, so that the voltage between the two surfaces can be computed by using

$$V = \int E_y dy$$

Similarly, the horizontal x-directed H-field probes are located along an x-directed line at the surface of the upper metal plate. This extends a couple of pin periods wider than the ridge on both sides of it, so that the total current can be computed from

$$I = \int H_x dx$$

Finally, the characteristic impedance of the gap waveguide becomes

$$Z_c = V / I$$

c) *P/I^2 model:* The E- and H-field distribution is computed over the whole cross section of the gap waveguide in the xy-plane, and the characteristic impedance is then computed from the total transmitted power *P* by

$$Z_c = P / |I|^2 \quad \text{with} \quad P = \iint\limits_{xy-plane} \mathrm{Re}\left\{E_y H_x^* - E_x H_y^*\right\} dxdy$$

Some results are shown in Table 1 and Fig. 3. They were evaluated for the final gap waveguide dimensions shown in Fig. 4d. For the ideal gap waveguide in Fig. 2b the computed characteristic impedance is very close to the theoretical 83 Ω value obtained from (1), see Table 1. This means that the V/I calculation model has been implemented correctly, and therefore should be correct also for the real gap waveguide. The WP model is not

believed to be correct for the real gap waveguide case as already discussed. The characteristic impedances of the ideal and real gap waveguide cases differ quite much when evaluated by the more correct V/I model, by around 30%, which can be a realistic effect of the actual ridge and periodic pin geometries used. However, for the real waveguide case the characteristic impedance computed by the V/I model shows a periodicity when plotted as a function of frequency. This is probably caused by the periodicity of the pin surface itself. The P/I^2 model was also used and gave similar results, but is much more time consuming and will be studied in more detail later. The preliminary conclusions so far is that there is really a need for having access to ports in longitudinally-periodic guiding structures when analyzing gap waveguides. We should mention here that we initially believed we designed the ridge for 50 Ω, but the present detailed analysis show that we did not succeed in that, which also show up in the results to follow. Therefore, we finally ended up with designing a TRL calibration kit to de-embed the bent gap waveguide itself.

4. Designing Pin Surface for Desired Parallel-plate Stopband in Dispersion Diagram

The characteristics of the gap waveguide are most clearly seen from its dispersion diagram. The most important is to determine the lower and upper cut-off frequency of the stopband. These cut-off frequencies can then be studied as a function of the geometrical parameters of the periodic surface geometry, and the gap height, in order to find a good solution. Such a study has already been reported for some parallel-plate geometries in [4], including the pin surface. Therefore, we have here chosen dimensions from results in [4] in order to cover 10-20 GHz, and we have computed the different dispersion diagrams for these dimensions. All the results have been obtained by the Eigen-mode Solver of CST and are shown in Fig. 4a-c. There exist also approximate analytical formulas for the lower and upper cut-off frequencies of the stop band of the pin surface [26], but these are only valid asymptotically for small period.

The computed dispersion diagrams in Figs. 4a (infinite periodic structure) and 4b (finite dimensions in transverse plane with PEC sidewalls) are computed without ridge and show a large stopband above 10 GHz where no waves can propagate. The left curve in Fig. 4a shows first the basic parallel-plate mode that starts at zero frequency as a TEM mode, and then it deviates from the light line and goes into cut-off slightly below 10 GHz. It appears again at 23 GHz, together with another mode. When we limit the transverse extent of the parallel-plate geometry by metal walls, as shown in Fig. 4b, several rectangular waveguide type modes appear below 10 GHz. They have a lower cut-off similar to normal rectangular waveguide modes, but go into a stopband slightly below 10 GHz, and they appear

again at the end of this parallel-plate stopband at 21 GHz.

The diagram in Fig. 4c includes the ridge as well. We see that the main difference compared to the diagram without ridge is that there is a new mode following very closely the light line within the whole parallel-plate stopband. This is the desired quasi-TEM mode following the ridge. We also see that the rectangular waveguide modes below 10 GHz are modified a bit by the ridge. There is also a new second mode coming in at 19 GHz. This is a higher order gap waveguide mode, having a vertical E-field distribution with asymmetric sinusoidal dependence across the ridge, being zero in the middle of the ridge. In comparison the vertical E-field distribution of the desired quasi-TEM mode is nearly constant across the ridge.

We have also for completeness computed the cavity resonances within a gap waveguide cavity with pins and surrounding metal wall. Then, we could also clearly see that the cavity resonances did not appear within the parallel-plate stopband 10-23 GHz.

5. Lateral Decay of Modal Field

It is of interest to know how fast the modal field decays laterally away from the ridge. This is computed in [26] using a plane wave spectral domain approach, and formulated analytically in [27]. The formulations are in both papers based on using the homogeneous surface impedance model for the pin surface developed in [11]. The two papers show lateral E-field decays in the order of 50 – 100 dB/λ, depending on dimensions and frequency. Our results computed by CST in the middle of the gap are shown in Fig. 5. The field varies periodically due to the periodicity of the pins (which are also shown along the abscissa). We see that above 15 GHz the maximum levels of the vertical E-field are down by 60 dB at a point located 20 mm (1 λ at 15 GHz) away from the edge of the ridge. Thus, the field decays strongly into the pin region also for our practical realization with finite pin period. The horizontal E-field component is also shown, and we see that this has a maximum in between the pins, due to the dominant TEM mode there [27].

6. Design of Demonstrator with Two 90° Bends and Coaxial Transitions

We wanted to design a demonstrator which was a bit more complicated than a simple straight transmission line, in order to be sure that the guiding properties of the gap waveguide could not be questioned. Therefore, we chose a line with two 90° bends. The bends were designed simply by a sharp inner 90° corner, whereas the outer ridge edge was metered, i.e. cut 45° in such a way that the cut triangle has two sides of the same length as the width of the ridge,

which is the common approach when designing microstrip bends.

We then designed two coaxial transitions to enable measurements with a normal VNA with coaxial ports. The simplest mechanical solution was to use coaxial connectors intended for being mounted on ground planes, to mount them to the top metal plate, and to let the inner conductor penetrate through the lid, via the gap and into a hole in the ridge, and thereby couple capacitively to the quasi-TEM gap waveguide mode. Thereby, we avoided any conductive contact to the ridge, and could keep the advantage of the simple mounting of the top plate inherently present with the gap waveguide technology. The dimensions and the resulting reflection coefficient S_{11} of a single transition are shown in Fig. 6. The length of the stub behind the hole in the ridge is about $\lambda/2$ at 15 GHz, measured from the middle of the hole. Thereby, the open line transforms to an open at the probe location in the middle of the ridge. The S_{11} computations were performed with a radiating boundary condition (termination) at the opposite end of the ridge.

7. Computed and Measured Results of Demonstrator

The whole gap waveguide demonstrator was computed between the two coaxial ports in order to simulate the S-parameter measurements. We also plotted the vertical E-field distribution at the surface of the upper smooth plate at some selected frequencies, shown in Fig. 7. The results clearly show the effect of the parallel-plate stopband. Below the 10 GHz lower cut-off frequency, the field spreads out over the whole width of the gap. Between 10 and 22 GHz the field is seen to follow the ridge via the two 90° bends. The confinement is particularly good between 13 and 18 GHz. At 19 GHz and above there is a strong standing wave along the ridge, due to a large mismatch. This is caused by the appearance of the second (asymmetric) gap mode at about 19 GHz, but also by the frequency limitations of the coaxial transition used. The computed S_{11} of the coaxial transitions were shown in Fig. 6. Also, the SMA coaxial connectors used are not specified for use above 18 GHz.

The computed and measured S-parameters are shown in Fig. 8. The performance is good between 13 and 17 GHz, and in agreement with what can be expected based on the return loss of the coaxial transitions. Below 12 GHz and above 18 GHz the performance is very bad, the latter beings already explained. The measured results showed in addition deviations up to 0.7 dB between S_{21} and S_{12} between 13 and 16.3 GHz, which is an indication of the measurement accuracy (they should have been identical). The absolute values of S_{11} and S_{22} were very similar, and in a lossless network they should be identical. We have in Fig 9 plotted S_{21} and S_{11} again, but now together with S_{21} and S_{11} of the long straight gap waveguide in the calibration kit in Sec. IX. We can identify the difference between the

curves as being due to the increased reflection level of the bent gap waveguide. The mismatch corrected transmission factor $e = |S_{21}|^2 / (1 - |S_{11}|^2)$ was calculated for both these cases, showing values around -0.2 dB. This value represents the total efficiency due to absorption in the two coaxial transitions and the ridge gap waveguide. We are not able to determine how much is due to the gap waveguide itself from these measurements. Therefore, we developed a gap waveguide TRL calibration kit.

8. TRL CALIBRATION KIT

In order to measure the S-parameters of the gap waveguide circuit itself, not including the coaxial transitions, we designed a TRL calibration kit in gap waveguide technology. This is described briefly below. The TRL calibration kit is shown in Fig. 10. It consists of one "short" realized by a shorting post that is assured to have good conductive contact to the lid by means of an extra screw into the post, one "thru" having the double length of the shorted line, and a "line" that is 6.5 mm longer than the thru. This value was chosen because it is exactly one pin period, corresponding to being $\lambda/4$ longer at 11.54 GHz. The calibration kit should therefore work best around 11.5 GHz and degrade towards 23 GHz when the length difference is $\lambda/2$. All coaxial transitions were made equal to the ones of the gap waveguide demonstrator. At first the calibrations were done up to the VNA ports using the SOLR-algorithm. Then measurements were done for the different standards such as Thru, Reflect and Line. After that, these measurement results were processed by commercially available software (based on TRL calibration concept), using the length difference of 6.5 mm between the thru and the line, and assuming that the gap waveguide had phase velocity equal to the free space velocity. Thus, no correction for the actual dispersion curve was used, Finally, the calibrated S-parameters were obtained. The calibration kit in Fig. 10 also include a long line, being 10 pin periods longer than the thru, i.e. 65 mm longer.The resulting calibrated S-parameters of both the demonstrator in Fig 1 and the long line of the calibration kit are shown in Fig. 10. We see that now the S_{11} of the straight line is 20 dB down over most of the frequency band, so that the calibrations have worked down to a level of -20 dB. The demonstrator with the two 90° bends have larger S_{11}, but it is still below –13 dB over most of the band. This is quite a reasonable value compared to microstrip bends. We have also calculated the mismatch corrected transmission factor in (1) for both the calibrated and uncalibrated gap waveguide circuits. The results are shown in Fig. 11.

We see that the mismatch corrected transmission factor (efficiency) is improved from -0.2 dB with coaxial

transmissions to almost 0 dB without the coaxial transmissions. Actually, the curves show even a gain up to 0.1 dB, meaning that our measurement accuracy is not better than that. Also, we see no significant difference between the straight and bent gap waveguides, meaning that the additional losses due to the two extra 90° bends are negligible. Therefore, the main conclusion of this is that the loss in the gap waveguide is so small that we need further and more accurate studies in order to determine it.

9. CONCLUSION

We have demonstrated that the newly introduced ridge gap waveguide works as a quasi-TEM transmission line by designing and measuring a demonstrator with a textured metal plate consisting of a ridge with two 90° bends, surrounded by metal pins that create the required parallel-plate stopband. The demonstrator works between 13 and 17 GHz with 0.3 dB insertion loss including two coaxial transitions and two 90° bends. We also designed a TRL calibration kit in gap waveguides, and showed that the 0.2 dB loss could be attributed to the two coaxial transitions. The remaining loss in the two 90° bends and intermediate gap waveguide is negligible. This was also confirmed by measuring a piece of straight gap waveguide of 65 mm length. The losses are so small that later more accurate studies are needed to determine them.

The frequency band limitation is mainly due to the mismatch of the coaxial transitions, but also because a second ridge gap mode appears at around 19 GHz, and because the coaxial connectors are not usable above 18 GHz. The useful bandwidth can easily be improved by a reduction of the ridge width, in which case the gap height must be reduced to keep the characteristic impedance the same, and by changing the transitions. The chosen pin dimensions have a theoretical parallel-plate stopband between 10 and 23 GHz, which is a definite of the available bandwidth. However, it could be possible to increase the bandwidth further by fine-tuning the periodic pin dimensions to a larger degree than this is already done in [10], and definitely this is possible by using other forms of high impedance surfaces such as mushroom surfaces, as also studied in [10].

The texture of the lower surface has dimensions of about 5 mm (pin length and thickness). This is easily manufactured, and it can even be easily manufactured when scaled to higher frequency. It should be possible to manufacture texture of dimensions 0.1 mm, which scales by a factor of 50 from the present demonstrator, meaning that we should be able to reach 20 GHz x 50 = 1 THz. Thereby, the mechanical simplicity makes the ridge gap waveguide an interesting transmission line for realizing components and circuits up to THz, including integration of

active components like MMICs and packaging. In order to be able to design gap waveguide components and show their usefulness up to THz, there is a need for further studies, such as to determine accurately the low ohmic losses, develop more complete analytical models and explanations including better results for characteristic impedances, develop good port models for use in general electromagnetic solvers, develop Green's functions for efficient analysis by moment method, design critical components, demonstrate integration of MMICs, develop alternatives to connecting MMICs by bonding (better adopted for the gap waveguide geometries), and to develop numerical approaches for analyzing whole MMIC circuits in a way that is compatible with FDTD and moment method solvers.

Finally, it should be mentioned that we have been made aware of that similar pin structures inside normal rectangular waveguides have been used to realize microwave filters in the past, being referred to as waffle-iron filters [27].

ACKNOWLEDGEMENTS

The authors want to acknowledge discussions with Z. Sipus, H. Zirath and S. Maci, and we are thankful to Mattias Ferndal for help with the TRL calibrations. We also want to thank to thank Dr. Miroslav Pantaleev from Onsala Space Observatory and Radio and Space Science Department of Chalmers regarding the manufacturing of the gap waveguide demonstrator and the TRL calibration kit.

REFERENCES

[1] P.-S. Kildal, E. Alfonso, A. Valero-Nogueira, E. Rajo-Iglesias: "Local metamaterial-based waveguides in gaps between parallel metal plates", IEEE Antennas and Wireless Propagation letters (AWPL), Volume 8, pp. 84-87, 2009.

[2] P.-S. Kildal: "Three metamaterial-based gap waveguides between parallel metal plates for mm/submm waves", 3rd European Conference on Antennas and Propagation (EuCAP 2009), Berlin, Germany, 23-27 March 2009.

[3] P.-S. Kilda:, "Waveguides and transmission lines in gaps between parallel conducting surfaces", European patent application EP08159791.6, July 7, 2008.

[4] E. Rajo-Iglesias, A. Uz Zaman, P.-S. Kildal: "Parallel plate cavity mode suppression in microstrip circuit packages using a lid of nails", accepted for publication in IEEE Microwave and Wireless Components Letters, August 2009.

[5] P.-S. Kildal: "Artificially soft and hard surfaces in electromagnetics", IEEE Trans. Antennas Propagat., Vol. 38, No. 10, pp. 1537-1544, Oct. 1990.

[6] A. Valero-Nogueira, E. Alfonso, J. I. Herranz, P.-S. Kildal: “Experimental demonstration of local quasi-TEM gap modes in single-hard-wall waveguides”, IEEE Microwave and Wireless Components Letters, Vol. 19, No. 9, pp. 536-538, Sept. 2009.

[7] E. Lier: “Analysis of soft and hard strip-loaded horns using a circular cylindrical model”, IEEE Transactions on Antennas and Propagation, Vol 38, No.. 6, pp. 783-793, June 1990.

[8] P.-S. Kildal and A. Kishk: “EM Modeling of surfaces with STOP or GO characteristics - artificial magnetic conductors and soft and hard surfaces”, Applied Computational Electromagnetics Society Journal, Vol. 18, No. 1, pp. 32-40, March 2003.

[9] D. Sievenpiper, L.J. Zhang, R.F.J Broas, N.G. Alexopolous, E. Yablonovitch: “High-impedance electromagnetic surfaces with a forbidden frequency band”, IEEE Transactions on Microwave Theory and Techniques, Vol. 47, No.11, pp. 2059-2074, November 1999.

[10] E. Rajo-Iglesias, P.-S. Kildal: “Cut-off bandwidth of metamaterial-based parallel plate gap waveguide with one textured metal pin surface”, 3rd European Conf. Antennas Propagat. (EuCAP 2009), Berlin, Germany, 23-27 March 2009. (will be replaced by submitted article if it is accepted)

[11] M. G. Silveirinha, C. A. Fernandes, J. R. Costa: “Electromagnetic characterization of textured surfaces formed by metallic pins”, IEEE Trans. Antennas Propagat., Vol. 56, No. 2, pp. 405-415, Feb. 2008

[12] I.V. Lindell: “Ideal boundary and generalised soft and hard conditions”, IEE Proceedings – Microwaves, Antennas and Propagation, Vol 147, No. 6, pp. 495-499, December 2000.

[13] A. Valero-Nogueira, E. Alfonso, J.I. Herranz, M. Baquero: “Planar slot-array antenna fed by an oversized quasi-TEM waveguide”, Microwave Opt. Technol. Lett., vol. 49, no. 8, pp. 1875–1877, Aug. 2007.

[14] J. M. Fernández, P. Padilla de la Torre and M. Sierra-Castañer: "Articial magnetic conductors enhancing the wave propagation in oversized parallel plate waveguide for planar antenna applications", Proceedings of the European Microwave Association; Special Issue on Microwave Metamaterials: Theory, Fabrication and Applications, vol. 2, no. 1, pp. 22-29, March 2006.

[15] E. Alfonso, P.-S. Kildal, A. Valero, and J. I. Herranz: “Study of local quasi-TEM waves in oversized waveguides with one hard wall for killing higher order global modes”, IEEE International Symposium on Antennas and Propagation (IEEE AP-S), San Diego, July 2008.

[16] Z. Sipus, H. Merkel and P-S. Kildal: “Green's functions for planar soft and hard surfaces derived by asymptotic boundary conditions”, IEE Proceedings Part H, Vol. 144, No. 5, pp. 321-328, Oct., 1997.

[17] CST Microwave Studio 2008. Available at: www.cst.com.

[18] M. Ng Mou Kehn and P.-S. Kildal:“Miniaturized rectangular hard waveguides for use in multi-frequency phased arrays”, IEEE Transactions on Antennas and Propagation, vol. 53, no. 1, pp. 100-109, Jan 2005.

[19] M. Ng Mou Kehn, M. Nannetti, A. Cucini, and S. Maci: "Analysis of dispersion in dipole-FSS loaded hard rectangular waveguide", IEEE Transactions on Antennas and Propagation, vol. 54, no. 8, pp. 2275-2282, Aug 2006.

[20] W. F. McKinzie: "Circuit and method for suppression of electromagnetic coupling and switching noise in multilayer printed circuit boards", US Patent No. 7,215,007 B2, May 8, 2007.

[21] A. Grbic, G.V. Eleftheriades: "Periodic analysis of a 2-D negative refractive index transmission line structure", IEEE Trans. Antennas Propagat., Vol. 51, No. 10, pp. 2604-2611, Oct. 2003.

[22] George V. Eleftheriades, Keith G. Balmain: "Metamaterials for controlling and guiding electromagnetic radiation", US Pat. 6859114 - Filed Jun 2, 2003.

[23] J.M. Schellenberg: "CAD models for suspended and inverted microstrip", IEEE Trans. Microwave Theory and Techniques, Vol.43, No.6, pp.1247-1252, June 1995.

[24] T. N. Anderson: "Rectangular and ridge waveguide", IEEE Trans. Microwave Theory and Techniques, Vol.4, No.4, pp. 201-109, Oct 1956.

[25] David Pozar: *Microwave engineering 3rd edition*, p. 139, Wiley, 2005

[26] Z. Sipus, P. Klokoc and P.-S. Kildal:"Local wave Green's functions of parallel plate metamaterial-based gap waveguides with one hard wall", 3rd European Conference on Antennas and Propagation, Berlin, Germany, 23-27 March 2009.

[27] S. Maci, A. Polemi, P.-S. Kildal: "Dispersion characteristics of a metamaterial-based parallel plate ridge waveguides", 3rd European Conference on Antennas and Propagation (EuCAP 2009), Berlin, Germany, 23-27 March 2009

[28] E. D. Sharp: "A high-power wide-band waffle-iron filter", IEEE Trans. MTT, Vol. 11, No. 2, pp. 111-116, March 1963

LIST OF FIGURE:

1) Photo of the 12-18 GHz demonstrator
2) Cross-sections of a) ideal linearly polarized hard waveguide, b) ideal gap waveguide, and c) stripline
3) Characteristic impedance of ridge gap waveguide
4) Different dispersion diagrams related to the ridge gap waveguide
5) Modal field of gap waveguide in transverse xy-plane computed with PMC sidewalls
6) Geometry and computed S_{11} of single coax to ridge gap waveguide transition
7) Computed vertical E-field distribution
8) Computed and measured S_{21} transmission coefficient between the two coaxial connectors of the ridge gap waveguide

9) S-parameters of bent ridge gap waveguide demonstrator in Fig. 1and the straight gap waveguide measured on their coaxial ports.
10) S-parameter results for the bent gap waveguide demonstrator in Fig. 1 and straight gap waveguide, obtained by using the TRL calibration kit in gap waveguide shown above
11) Insertion loss for the 2 cases after taking away the mismatch effect

FIGURES:

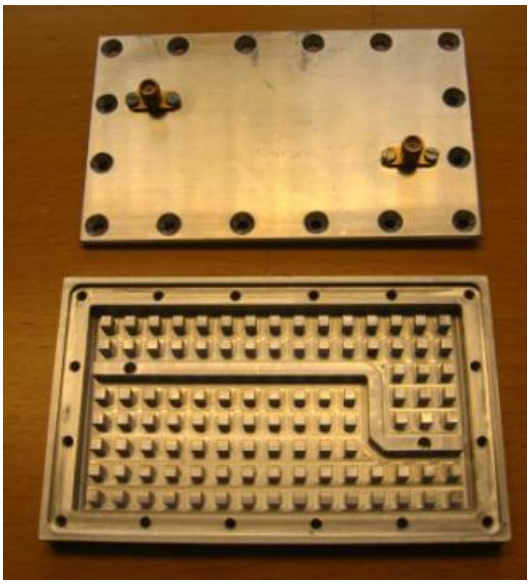

Figure 1: Photo of the 12-18 GHz demonstrator designed and measured for verifying the ridge gap waveguide technology. The upper plate is removed to reveal the textured plate, showing the guiding ridge surrounded by metal pins.

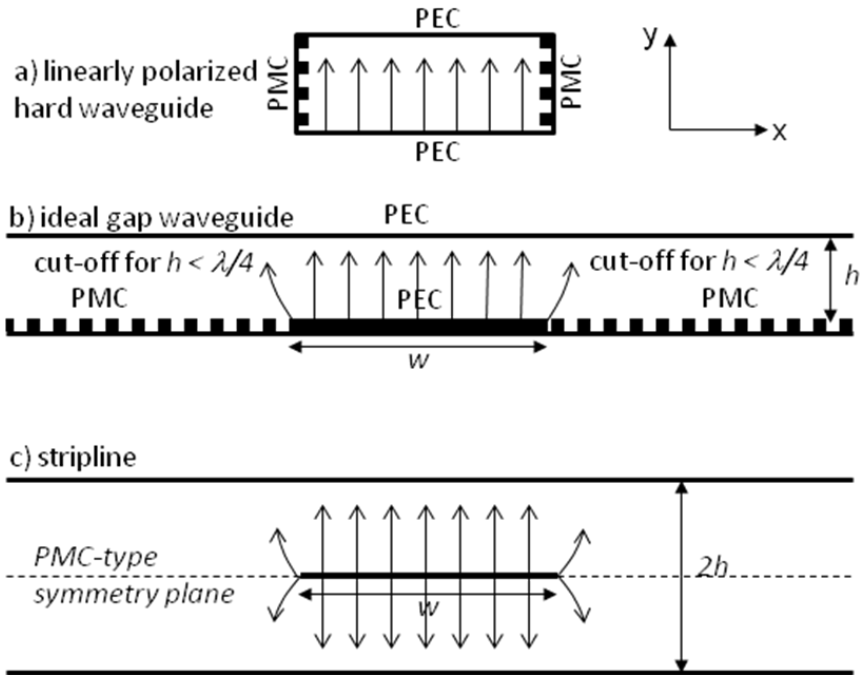

Figure 2: Cross-sections of a) ideal linearly polarized hard waveguide, b) ideal gap waveguide, and c) stripline.

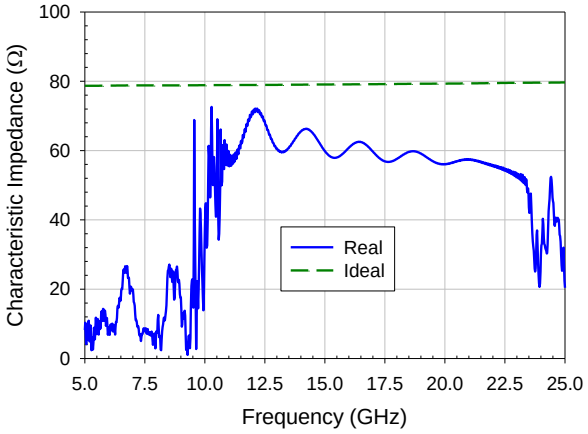

Figure 3: Characteristic impedance of ridge gap waveguide calculated by the described V/I model from field simulations using CST, both for the ideal PEC/PMC gap waveguide (dashed) and the real ridge gap waveguide with surrounding pins (solid).

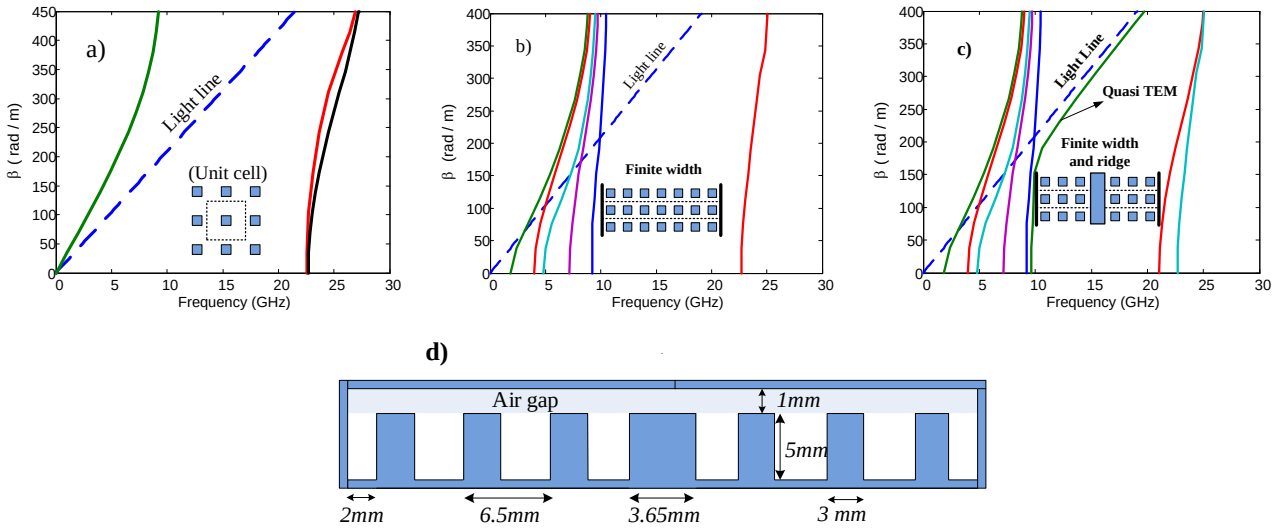

Figure 4: Different dispersion diagrams related to the ridge gap waveguide surrounded by pins, a) Infinite parallel-plate structure wherein one plate has periodic pin surface without metal ridge. b) Same as in a, but finite parallel-plate structure with seven rows of pins and metal sidewalls. c) Same as in b, but with metal ridge instead of the central row of pins. d) Dimensions of pin surface in cross-sectional xy-plane with ridge of width *3.65 mm*, gap height of *1 mm* and pins.

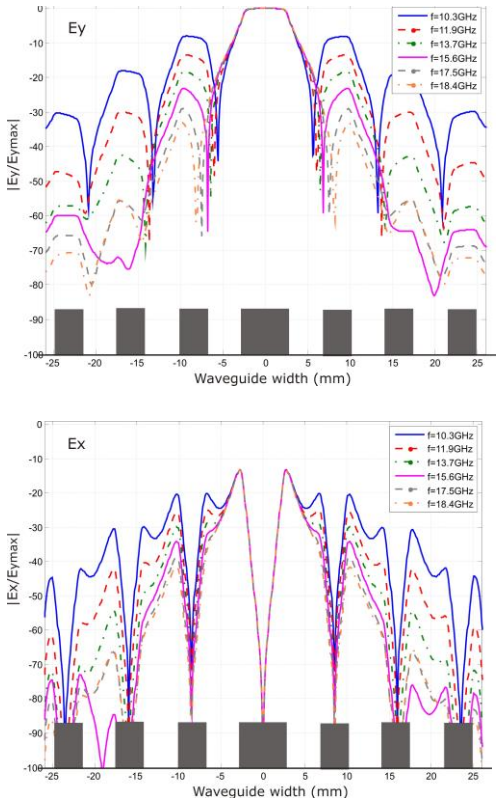

Figure 5: Modal field of gap waveguide in transverse xy-plane computed with PMC sidewalls for geometry in Figure 3 c. The upper graph is from [1].

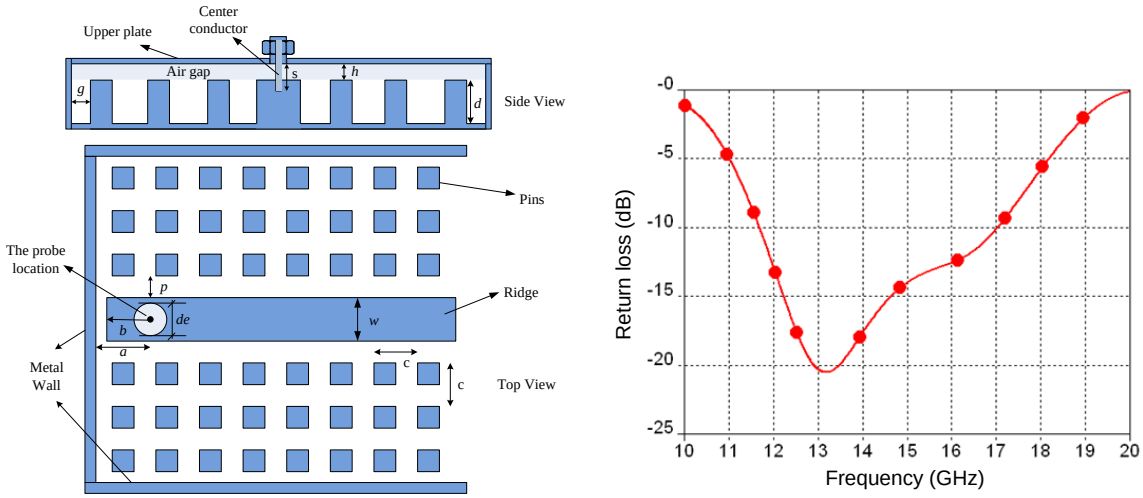

Figure 6: Geometry and computed S_{11} of single coax to ridge gap waveguide transition. The dimensions are s = 3.75 mm, d = 5 mm, b = 10 mm, a = 12mm, p = 3.5mm, h= 1mm, w = 3.65*mm*, *de= 3.45mm*, g =2mm, c = 6.5 mm. The size of the surrounding box did not affect the results.

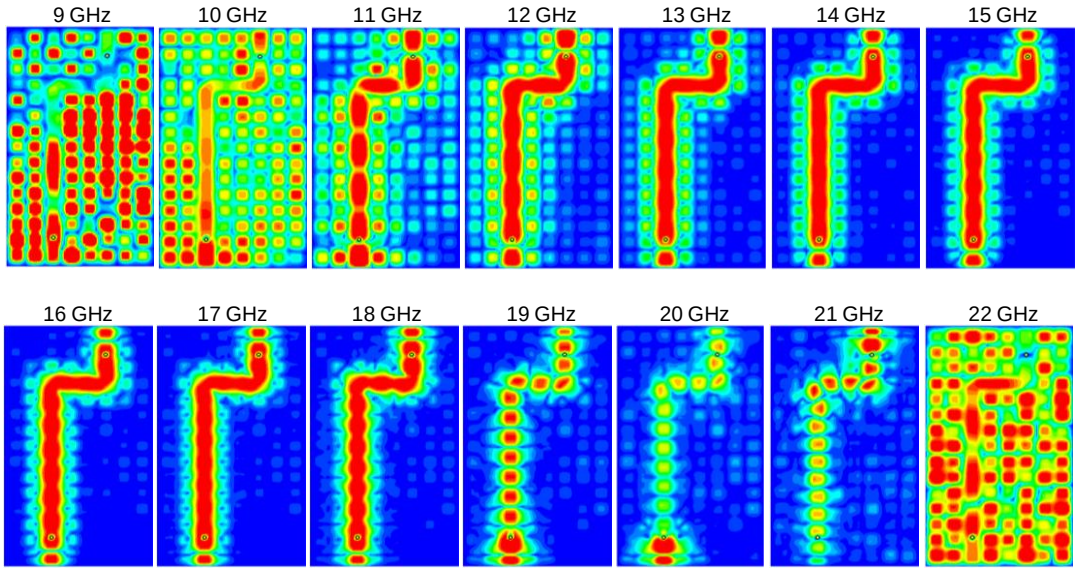

Figure 7 : Computed vertical E-field distribution at the surface of the upper smooth metal plate of the demonstrator in Fig. 1 at selected frequencies. The color scale covers distribution variations between high (black) and zero or low (white) values.

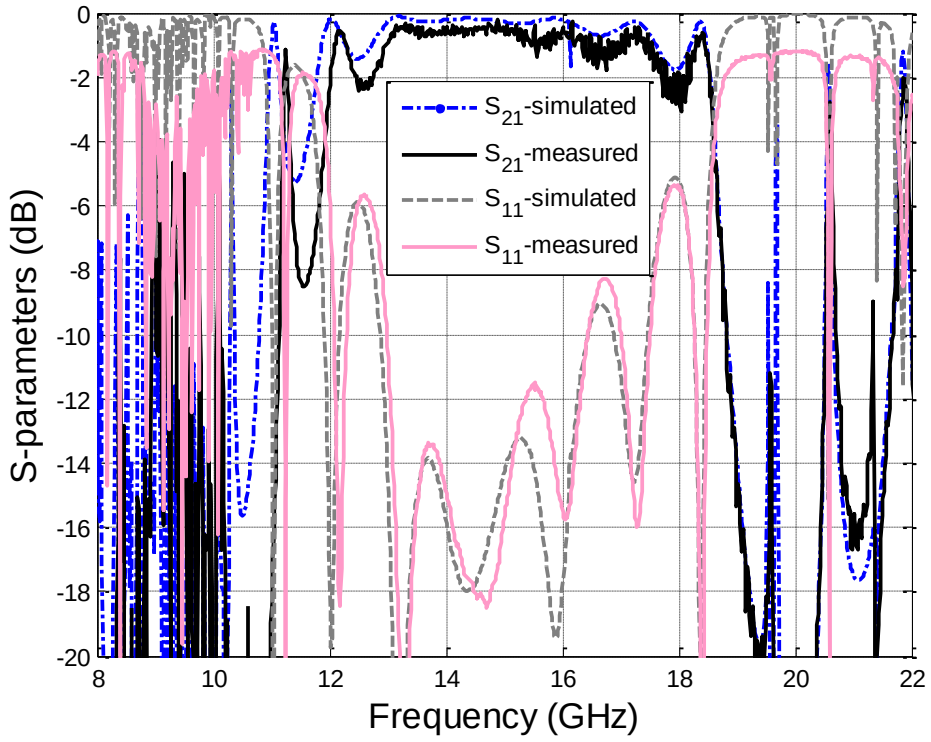

Figure 8: Computed and measured S_{21} transmission coefficient between the two coaxial connectors of the ridge gap waveguide demonstrator in Fig. 1.

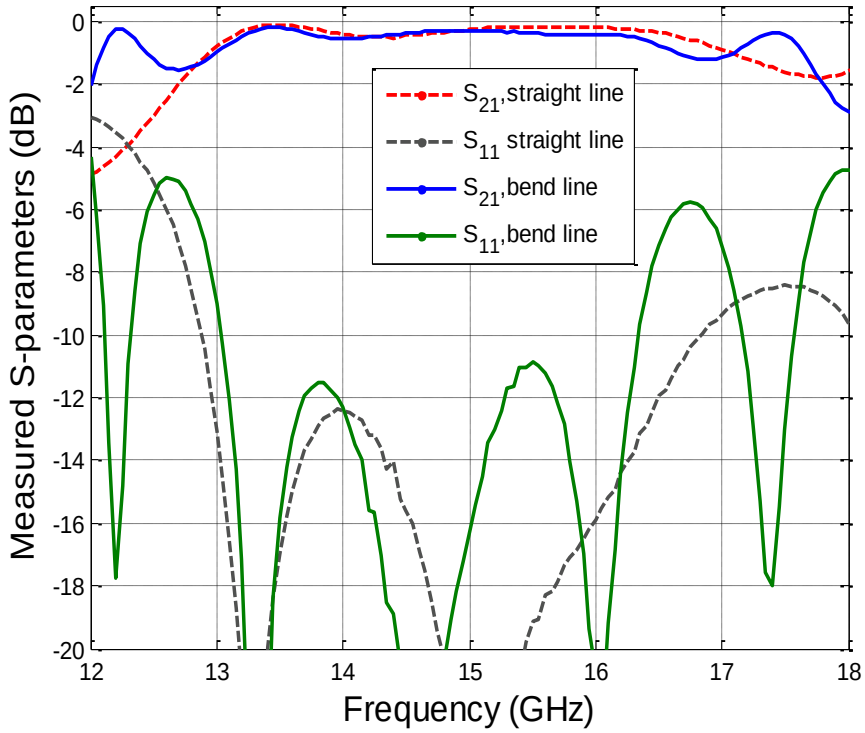

Figure 9: S-parameters of bent ridge gap waveguide demonstrator in Fig. 1and the straight gap waveguide measured on their coaxial ports. The straight line is the "long line" shown in Fig. 10.

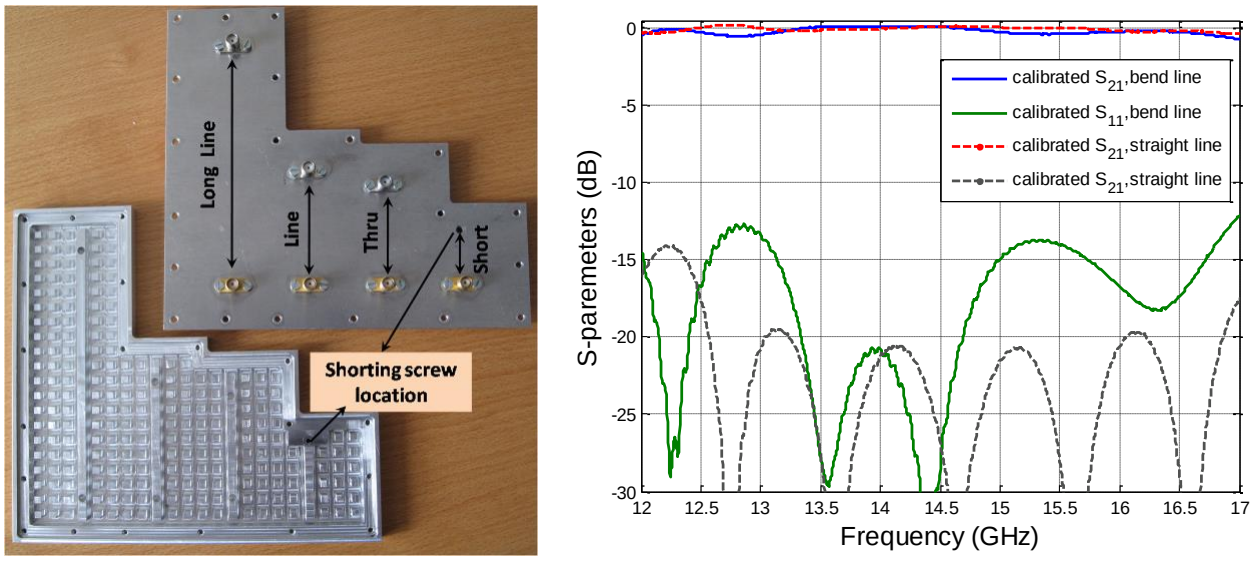

Figure 10: S-parameter results for the bent gap waveguide demonstrator in Fig. 1 and straight gap waveguide, obtained by using the TRL calibration kit in gap waveguide shown above. The straight line is the extra "long line" of the calibration kit.

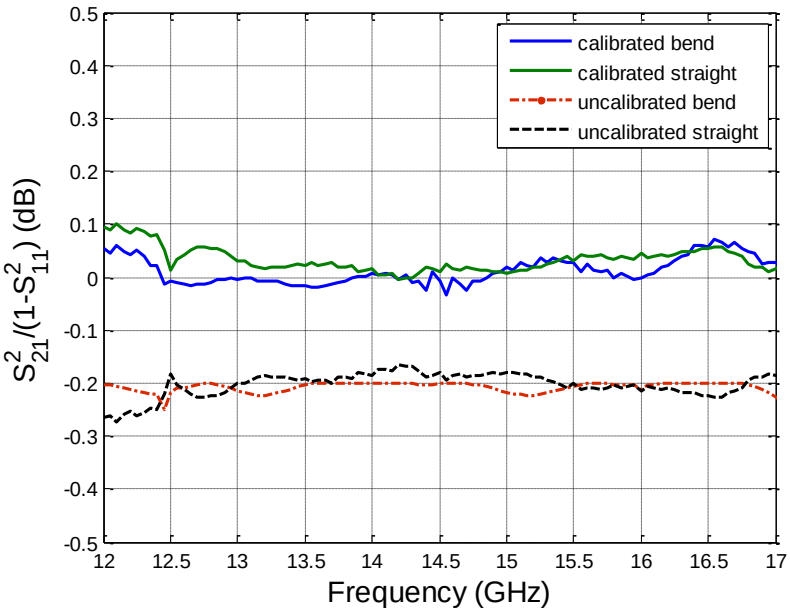

Figure 11: Insertion loss for the 3 cases after taking away the mismatch effect

Table:1 Characteristic impedance of ideal and real ridge gap waveguide computed by different models at 15 GHz.

Type	Stripline equivalent	Ideal gap waveg.		Real gap waveg.	
Model	Eq. (1)	WP	V/I	WP	V/I
Z_k	83Ω	82Ω	80Ω	78Ω	60Ω

Authors Information

Per-Simon Kildal (M'82-SM'84-F'95) has been Professor at Chalmers University of Technology, Gothenburg, Sweden since 1989 (**www.kildal.se**). He has authored antenna texbook, and 98 articles in IEEE or IET journals, two of which have received best paper awards. Kildal has designed two very large antennas, including the Gregorian dual-reflector feed of Arecibo radiotelescope. He has invented several reflector antenna feeds, the latest being the so-called "Eleven antenna". He is the originator of the concept of soft and hard surfaces. Kildal's research group has pioneered the reverberation chamber into an accurate measurement tool for antennas and wireless terminals subject to Rayleigh fading.

Ashraf Uz Zaman was born in Chittagong, Bangladesh. He received his BSc. in Electrical and Electrical Engineering from Chittagong University of Engineering and Technology, Bangladesh in 2001. In 2007, he received his MSc. degree from Chalmers University of Technology, Sweden .At present, he is with the Signal Processing and Antenna division of same university and is working towards his PhD. His main research interest includes millimeter and sub millimeter waveguide technology, frequency selective surfaces, integration of MMIC with the antennas etc.

Eva Rajo-Iglesias (S'97-M'02) was born in Monforte de Lemos, Spain, in 1972. She received the Telecommunication Engineering degree from University of Vigo, Vigo, Spain, in 1996 and the Ph.D. degree in Telecommunication from University Carlos III of Madrid, Madrid, Spain, in 2002. From 1997 to 2001 she was Teacher Assistant at the University Carlos III of Madrid. In 2001 she joined the University Polytechnic of Cartagena as Teacher Assistant for a year. She came back to University Carlos III as a Visiting Lecturer in 2002 and since 2004, she is an Associate Professor with the Department of Signal Theory and Communications at University Carlos III of Madrid. She has visited Chalmers University of Technology (Sweden) five times as

a guest researcher, during autumn 2004, 2005, 2006, 2007 and 2008 where she is now an Affiliated Professor in the Signals and System Department. Her main research interests include microstrip patch antennas and arrays, periodic structures and optimization methods applied to electromagnetics. She has (co)authored more than 30 contributions in international journals and more than 60 in international conferences. Dr. Rajo-Iglesias received the Loughborough Antennas and Propagation Conference (LAPC) 2007 Best Paper Award.

Esperanza Alfonso Alós received the degree in electrical engineering from the Polytechnic University of Valencia (UPV), Valencia, Spain, in 2004, and is currently working toward the PhD at UPV. She has been with the Institute of Telecommunications and Multimedia Applications of the UPV since 2004. Her main research interests include analysis and design of slot array antennas, numerical methods, millimiter and submillimiter waveguide technology and metamaterials**.**

Alejandro Valero-Nogueira (S'92–M'97) was born in Madrid, Spain, on July 19, 1965. He received the M.S. degree in electrical engineering from the Universidad Politécnica de Madrid, Madrid, Spain, in 1991, and the Ph.D. degree in electrical engineering from the Universidad Politécnica de Valencia, Valencia, Spain, in 1997. In 1992 he joined the Departamento de Comunicaciones, Universidad Politécnica de Valencia, where he is currently an Associate Professor. During 1999, he was on leave with the ElectroScience Laboratory, The Ohio State University, where he was involved in fast solution methods in electromagnetics and conformal antenna arrays. His current research interests include computational electromagnetics, Green's functions, waveguide slot arrays, hard surfaces and metamaterial-based waveguides.